Journal of Non-Crystalline Solids 356 (2010) 2928–2934

Contents lists available at ScienceDirect

Journal of Non-Crystalline Solids

journal homepage: www.elsevier.com/ locate/ jnoncrysol

Structural role of Zr^{4+} as a nucleating agent in a $MgO–Al_2O_3–SiO_2$ glass-ceramics: A combined XAS and HRTEM approach

Olivier Dargaud [a,b], Laurent Cormier [b], Nicolas Menguy [b], Laurence Galoisy [b], Georges Calas [b,*], Sophie Papin [a], Gilles Querel [c], Luca Olivi [d]

[a] Saint-Gobain Recherche, 39 Quai Lucien Lefranc, 93 303 Aubervilliers, France
[b] Institut de Minéralogie et de Physique des Milieux Condensés, Université Pierre et Marie Curie, CNRS UMR 7590, Université Paris Diderot, IPGP, 140 Rue de Lourmel, 75 015 Paris, France
[c] Saint-Gobain Northboro Research and Development Center, Goddard Road, Northborough, 01532-1545, MA, USA
[d] Elettra Sincrotrone Trieste S.C.p.A., Strada Statale 14, 34149 Basovizza, Trieste, Italy

ARTICLE INFO

Article history:
Received 24 February 2010
Received in revised form 2 April 2010
Available online 16 September 2010

Keywords:
Nucleation;
81.05.Kf=glasses;
61.43.Fs=glass;
EXAFS;
HRTEM;
Glass structure;
Vitroceramics

ABSTRACT

The environment around Zr^{4+} is studied at the Zr K-edge in a $MgO–Al_2O_3–SiO_2$ glass-ceramics heat treated along its very first crystallization steps. The heat treatments were calibrated by differential scanning calorimetry. ZrO_2 acts as a nucleating agent, adding a nucleation/crystallization event around 920 °C, less than 100 °C above the glass transition temperature (830 °C) and below the massive crystallization of the parent-glass (~1015 °C). It also lowers crystallization temperatures of the matrix as compared with a Zr-free sample. High-resolution transmission electron microscopy imaging allows an unambiguous attribution to tetragonal ZrO_2 for, at least, some of the very first detectable crystallites. Zr K-edge extended X ray absorption fine structure analysis shows a peculiar surrounding around Zr^{4+} in the parent glass, composed of Si (Mg,Al) and Zr sites linked by edge sharing. This indicates direct linkages between Zr sites, pre-existing in the glass structure that play a key role for promoting nucleation. This analysis is in agreement with only a small part of Zr^{4+} evolving during the first steps of nucleation toward the formation of few nano-crystals of tetragonal (ZrO_2).

1. Introduction

Glass-ceramics, discovered by S.D. Stookey in the mid-1950s [1], result from the nucleation and further crystallization of a parent-glass through a controlled thermal treatment [2,3]. Forming and shaping the parent-glass using glass manufacturing processes provide unique properties to the final material. Generally, nucleating agents, such as TiO_2 or ZrO_2 are used to promote bulk crystallization of nano-phases that serve as local heterogeneities for the crystallization of the desired phases. Phase separation on glass reheating prior to the occurrence of crystal nucleation has also been invoked [2,4]. The processes governing at the atomic scale the amorphous-to-crystal transformation around nucleating agents are essential to understand the formation of glass-ceramics but are still poorly understood.

Glass-ceramics in the $MgO–Al_2O_3–SiO_2$ (MAS) ternary system have been extensively studied due to the broad range of their applications [5–7]. Structural studies have concerned cordierite ($2MgO–2Al_2O_3–5SiO_2$) glasses containing Ti^{4+} or Cr^{3+} as nucleating agents [8,9] and SiO_2-rich MAS glasses ($MgO–1.21Al_2O_3–6.8SiO_2$) containing Zr^{4+} [10]. For instance, in Ti-bearing cordierite glasses, nucleation is favored by a preferential bonding between Al and Ti sites pre-existing in the initial glass [11]. However, little is known about the role and the interaction between the glassy matrix and the nucleating agent that will precipitate first.

Among the cations forming nucleating agents, zirconium has received some attention due to its importance for tailoring specific properties of glasses and glass-ceramics. Zr^{4+} has an important structural role in the glassy matrix. In alkali silicate and borosilicate glasses, Zr^{4+} occurs in octahedral coordination, with the ZrO_6 octahedra being corner-linked to SiO_4 tetrahedra [12]. This geometry favors the insertion of Zr^{4+} within the glassy matrix. Conversely, a recent study has shown the presence of a higher coordination number of Zr^{4+} in a MAS glass [13]. During the nucleation of MAS-Zr glasses, the first step is the nucleation/growth of nanocrystalline ZrO_2 that appears few degrees above the glass transition temperature (around 800 °C) [14]. In the same system, Zr^{4+} was reported to promote an amorphous phase separation with the formation of ZrO_2-rich regions of about 45 Å radius [15].

The present study concerns the nucleation of a Zr-bearing $MgO–1.21Al_2O_3–6.8SiO_2$ glass. Structural transformations were investigated in samples quenched after thermal heating treatments, the temperatures being chosen relative to the information provided by Differential Scanning Calorimetry (DSC). Transmission Electron Microscopy (MET) indicates the formation of well-crystalline ZrO_2 crystallites of

* Corresponding author.
E-mail address: georges.calas@impmc.upmc.fr (G. Calas).

0022-3093/$ – see front matter © 2010 Elsevier B.V. All rights reserved.
doi:10.1016/j.jnoncrysol.2010.05.104

Table 1
Parent-Glass Composition in wt.% probed by electron microprobe analysis.

Parent-glass	MgO	Al_2O_3	SiO_2	ZrO_2	Tot.
Zr-free	11.15	13.82	75.04	–	100
Zr-containing	10.21	13.82	72.14	3.84	100

few nanometers. Zr K-edge X-ray Absorption spectroscopy (XAS) data show a peculiar environment of Zr^{4+} in the parent-glass, Zr^{4+} occurring in 7-fold coordination surrounded by Si (Mg,Al) and Zr next-nearest neighbors in edge-sharing polyhedra. The presence of edge-sharing ZrO_7 polyhedra corresponds to a pre-organization of the glass that may favor the crystallization of ZrO_2 upon heating the parent-glass. There is only a small evolution of the local surrounding of Zr^{4+} during the first stages of nucleation. This demonstrates the major role played by the structural properties of Zr^{4+} as nucleating agent.

2. Experimental procedures

Glasses of compositions $(100-x)[MgO–1.21\ Al_2O_3–6.8\ SiO_2]+x\ ZrO_2$ with $x=0$ and 4, were prepared from high-purity compounds. Starting materials were ground together and melted in a Pt crucible at 1650 °C for 2 h. The glass was obtained by pouring the bottom of the crucible into water. The fusion, quenching and grinding were repeated twice to ensure homogeneity and glass composition was checked by electron microprobe analysis (Table 1).

Differential scanning calorimetry (DSC) measurements were performed on powdered parent-glasses (sieved at 50 μm), at the rate of 6 °C min^{-1} on a Setaram MultiHTC 96 up to 1600 °C, under N_2 flow. Thermal treatments were performed on the parent-glass heated at Tg and temperatures along the first exotherm measured by DSC. For that purpose, sound piece of glasses were heated at 838 °C, 909 °C, 920 °C, 932 °C and 944 °C in an electric furnace at a similar heating rate of 6 °C min^{-1} and quenched into deionized water.

High-Resolution Transmission Electron Microscopy (HRTEM) observations were performed using a JEOL 2100F microscope equipped with a field emission gun (200 keV) and a high-resolution UHR pole piece. Electron micrographs were obtained with a Gatan GIF 2001 and a Gatan US4000 CCD camera.

X-ray Absorption Spectroscopy (XAS) data were collected at Zr K-edge (17,998 eV) on the XAFS beam line of the ELETTRA synchrotron (Trieste, Italy) in transmission mode with a Si(111) monochromator and a 2 s/point integration time [16]. Incident (Io) and transmitted (It) X-ray intensities were measured using Ar filled ionization chambers. The beam size was approximately 8 × 3 mm. Each spectrum was calibrated with metallic Zr. Except for the Zr-containing parent-glass which consisted in a 1 μm polished slice of 1000 μm thickness, the XAS spectra of the glass-ceramics were measured on powdered samples mixed with an appropriate amount of boron nitride to match an absorption step of ~1. An average of 8 spectra was measured at 77 K in a liquid nitrogen cryostat (except for the parent-glass and the sample heated at 936 °C, with an average of 4 spectra).

Reference compounds include Y-doped tetragonal zirconia (t-ZrO_2)[1] and baghdadite ($Ca_3ZrSi_2O_9$), for 8-fold and 6-fold coordinated Zr^{4+}, respectively. t-ZrO_2 contains less than 3% monoclinic ZrO_2 (m-ZrO_2). Baghdadite was synthesized following [17]. Each standard was verified by X-ray powder diffraction.

Extended X-ray Absorption Fine Structure Spectroscopy (EXAFS) data were analyzed using the GNXAS package [18,19]. The same background function has been subtracted for the XAS spectra of all samples. The multiple-electron excitation at around 18,220 eV is observed in crystalline references and glass-ceramics, with the same width of approximately 2–4 eV and same jump of 0.03 total absorbance. Its extraction was thus made under the same conditions. Although the fits are processed in the energy space, EXAFS are presented in the conventional k-space. The core-hole life-time correction factor and resolution factor were fixed to 0.0 and 1.8 eV, respectively (Si 111 monochromator resolution at Zr K-edge). The value of the intensity factor S_0^2 (0.75) and $E_0 = 18{,}012$ eV was determined from the fitting of reference spectra. In the two references used, the S_0^2 factor reaches values around 0.80–0.72, which is in accordance with the values found in literature [20,21]. The corresponding Fermi levels are at 18,012 and 18,010 eV for baghdadite and t-ZrO_2, respectively. The different contributions issued from the reference fitting were used to fit the glass-ceramic spectra. Distances, Coordination Numbers (CN) and variance (Debye Waller like term, in $Å^2$) for each contribution were fitted along a single minimization step with all structural and extraction parameters (e.g. spline coefficients). There is no significant evidence for multiple scattering events within the coordination shell such as Zr–O–Zr–O–Zr, by contrast to other glasses in which Zr occurs in highly symmetric octahedral sites [21]. The multi-electronic Zr $K,M_{4,5}$ excitation at ~18,220 eV [22,23] was modeled by an arctangent function. Errors where calculated as mentioned in [19].

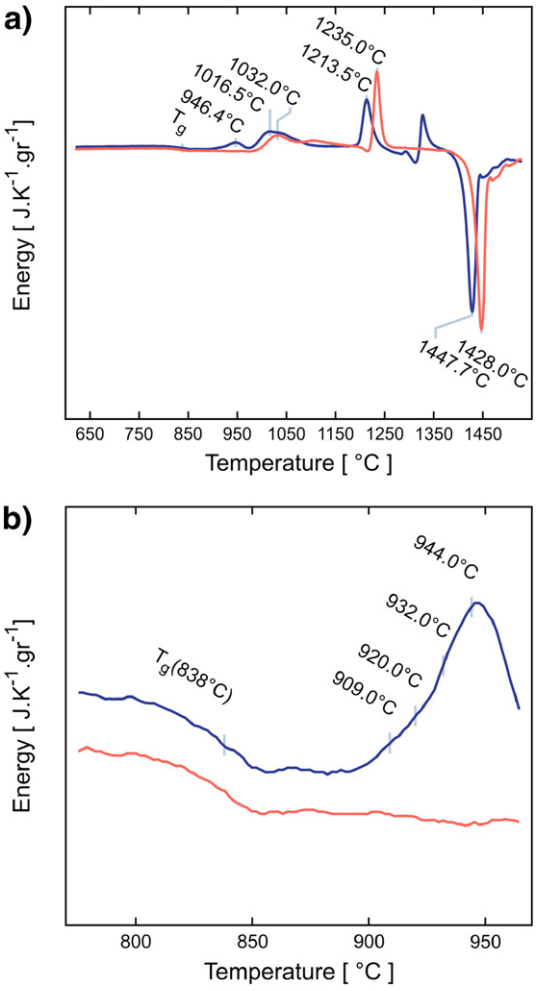

Fig. 1. a) Differential scanning calorimetry thermograms. Main events temperatures are reported on the plot. In grey the Zr-MAS, in violet Zr-free-MAS. b) The region of interest for the nucleation/first crystallization processes investigated in this study, ranging from Tg to the first DSC exotherm of the Zr-MAS parent-glass. The straight lines mark quenching temperatures of the samples used in this study (838 °C, 909 °C, 920 °C, 932 °C and 944 °C resp.).

[1] From Saint-Gobain ZirPro.

3. Results

3.1. DSC results

The DSC thermograms (Fig. 1a) of the two investigated compositions, with and without Zr, show significant differences, despite both glasses exhibit similar T_g values at 830 ± 1 °C. The Zr-containing parent-glass alone exhibits a first exotherm in the range ~890–970 °C, with a maximum at 946 °C, attributed to nano-ZrO_2 formation. At higher temperature, Zr-containing and Zr-free glasses exhibit similar thermal events shifted by −20 °C in the Zr-containing parent-glass. This emphasizes the macroscopic role of Zr^{4+} as nucleating agent: it lowers the temperature of crystallization(s) of the glass-ceramics [4]. The two events at ~1016 and 1213 °C arise from the crystallization of a β-quartz solid-solution $(MgO–Al_2O_3)_{1-\beta}–[SiO_2]_\beta$, (where $0.4<\beta<1$ [24]) and its transformation to cordierite [14,25] and $MgO–Al_2O_3$ spinels [26–28]. In those systems, magnesian petalite [29], osmulite [30] and zircon [25] are also reported and can crystallize in the case of slow heat treatment (heat rate below the Kelvin per min). Fusion occurs at 1428 °C and 1447 °C for the Zr-containing and Zr-free glasses, respectively. The glass-ceramics were obtained with the heat treatment temperatures represented in Fig. 1b.

3.2. HRTEM results

High-Resolution Transmission Electron Microscopy (HRTEM) observations show that the heat treatment does not produce any significant modification in the aspect of the glass matrix until 944 °C. No evidence of phase separation and no crystallites are observed by TEM and HRTEM up to 932 °C in the nm-resolution of the microscope. For the sample at 932 °C, the very first detectable nuclei appear with a size around 3–5 nm (Figs. 2 and 3) with a scarce density. The sample heated at higher temperature (944 °C) shows an increase in the density of crystals as well as an increase in their size (around 5–10 nm) (Fig. 3b). The dark field micrograph (Fig. 3c) is obtained by the selection of a diffraction spot of nano-phases embedded into the glass.

The Fourier transform of the HRTEM fringes (Fig. 3a and b) presents an axis zone compatible with the [100] direction of t-ZrO_2. The diffraction pattern shows the spot corresponding to the t-ZrO_2 012 planes. This reflection corresponds to the forbidden reflection 121 in cubic ZrO_2 (c-ZrO_2): the [100] direction of the $P4_2/nmc$ t-ZrO_2 lattice is equivalent to the [101] direction in the Fm3m cubic lattice [31]. The simulation of the diffraction pattern for t-ZrO_2 reproduces the experimental pattern (Fig. 3c). Moreover, these spots cannot result from an artifact due to a double diffraction. X-ray diffraction (XRD) cannot be as discriminative due to the broadening of the diffraction peaks of nano-phases and the closeness of lattice symmetry, which causes an overlap of the main diffraction peaks of c- and t-ZrO_2, as discussed by [32]. To our knowledge, this is the first report that the first nano-sized crystals can be unambiguously attributed to t-ZrO_2.

3.3. X-ray Absorption Near Edge Structure (XANES)

Zr K-edge XANES spectra are sensitive to the coordination and symmetry of the Zr-site, as shown for the crystalline reference spectra in Fig. 4. For baghdadite, the XANES spectrum shows a main edge which is split in two features B and C typical for 6-fold Zr (Fig. 4). For 8-fold Zr, the spectrum of t-ZrO_2 shows a more complex main edge and a characteristic feature at higher energy, near 18,045 eV.

The XANES spectra of the parent-glass and glass-ceramics treated up to 932 °C are similar, with a main edge which is split into two peaks, B and C, of similar and weak intensity (Fig. 4). These spectra are different from those found in other silicate glasses where Zr^{4+} occurs in regular 6-fold coordination [12,21]. They have been recently interpreted as indicating the presence of 7- or 8-fold coordinated Zr^{4+} sites, but remain distinct from the XANES spectrum of t-ZrO_2 [13]. In the parent-glass and glass-ceramics, the intensity of

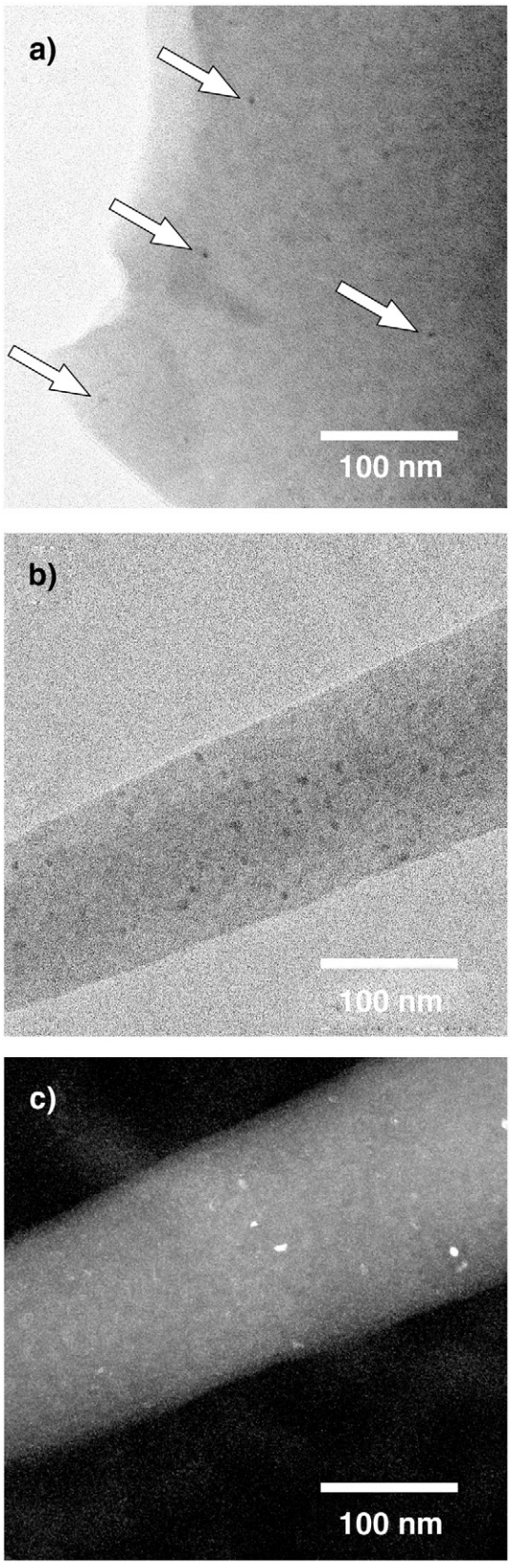

Fig. 2. TEM micrographs of the parent-glass and nucleated/crystallized samples. a) sample treated at 932 °C; b) sample treated at 944 °C. c) dark field image of zone b).

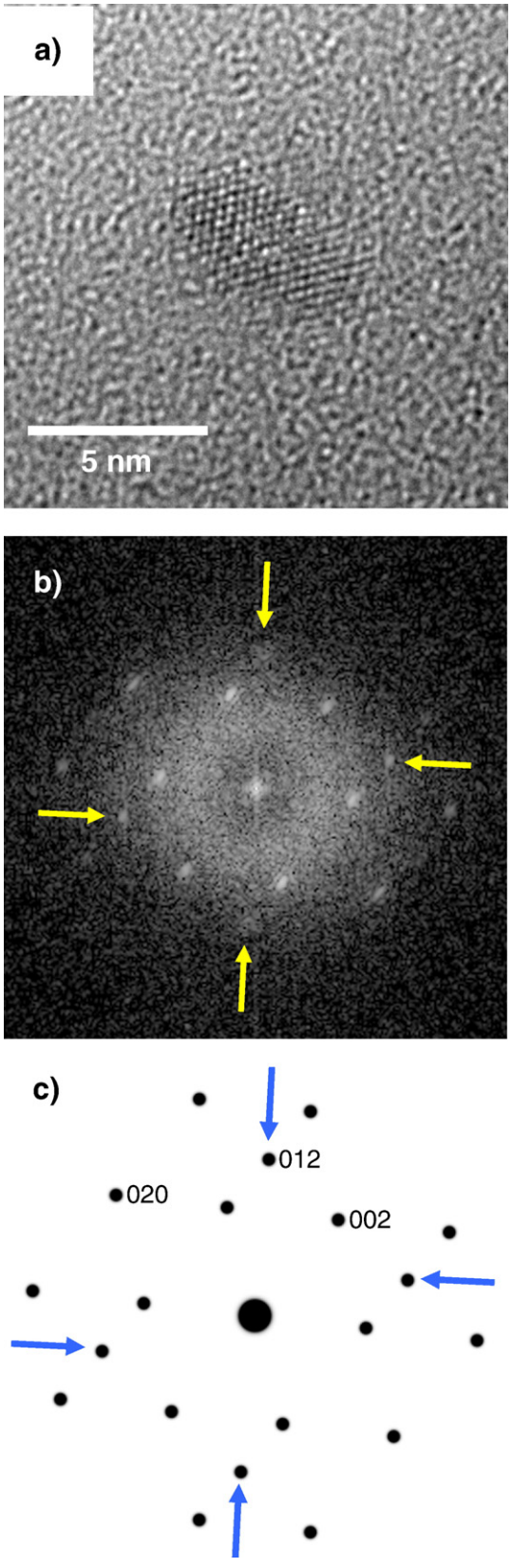

Fig. 3. a) High-Resolution micrographs of the sample heat treated at 932 °C; b) Fourier transformed images of the crystalline regions; c) simulated pattern of b). The spots corresponding to the 012 plane family are marked with arrows.

peak A remains constant and is more intense than usually observed in glasses [13,33,34]. This indicates a lack of center of symmetry of the Zr^{4+} sites in our glass and glass-ceramics.

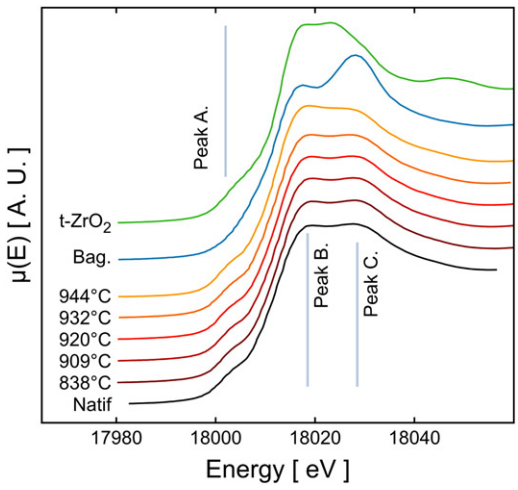

Fig. 4. XANES spectra of parent-glass and nucleated samples noted with their respective heat treatment temperatures along a 6 °C min^{-1} heat ramp. Reference samples baghdadite and Y-doped t-ZrO_2 are noted bag. and t-ZrO_2 respectively.

In the sample heated at 944 °C the intensity of peak B slightly increases as the peak C shifts toward lower energy. However, the spectrum remains different from that of t-ZrO_2.

3.4. Zr K-edge Extended X-ray Absorption Fine Structure (EXAFS)

EXAFS spectra of crystalline references were analyzed according to the Zr-surrounding [35,36]. The EXAFS model of the first oxygen shell in baghdadite includes a single contribution Fig. 5 with a high variance distribution (Table 2), in accordance with crystallographic data (distribution of Zr-O distances between 1.99 and 2.17 Å). The second shell contains two Si and one Zr contribution and 7 Ca, with broad distribution of Ca-Zr distances. A good fit is then obtained, with interatomic distances in good agreement with those determined by XRD (Table 2). However, the shortest Zr–Si contribution has a shorter value of 3.10 Å from EXAFS compared to 3.25 Å from XRD. EXAFS data of t-ZrO_2 are consistant with the literature [37,38]. The Zr–O shell corresponds to two contributions at 2.09 Å and 2.34 Å and the Zr–Zr contribution is found at 3.64 Å (2.10 and 2.33 Å, and 3.62 Å, respectively in [37]) (Fig. 6).

The structural model of the Zr environment in glass and glass-ceramics is built using the pair contributions (i.e., Zr–O, Zr–Zr and Zr–Si) calculated for baghdadite and t-ZrO_2. For the parent-glass, the first shell corresponds to a Zr–O contribution at 2.11 Å, with a high variance (around 0.019 $Å^2$) and no asymmetry factor. This distance is in accordance with 7-fold Zr^{4+} [39]. The number of neighbors given by the fit is around 7, in accordance with the indirect indications from XANES. More over a 7-fold site geometry may not present any center of symmetry in accordance with the intense pre-edge.

Second shell contributions correspond to Zr–Si (or Zr–Al, Zr–Mg) at 3.11 Å and Zr–Zr at 3.40 Å. The residual (i.e. the best fit subtracted to experimental) shows an oscillation having a small intensity relative to the data noise at high k, which is below all fitting contribution intensities in the low k part of the spectra. Zr–Si and Zr–Zr contributions are consistent with edge-sharing linkages such as Zr–Si = 2.98 Å in Zircon ($ZrSiO_4$) [40] and for an averaged Zr–Zr = 3.47 Å in m-ZrO_2 [41].

Zr–Si (Al, Mg) contributions mostly arise from Si, as the Al and Mg contents are smaller than the Si one. The high number of neighbors (Table 3) shows a well-ordered second shell around Zr^{4+} in the parent-glass. The Zr–Zr contribution represents a number of neighbors around 1 with a variance around 0.009 $Å^2$. The small distances could not be interpreted as multiple scattering that would necessarily imply higher distances.

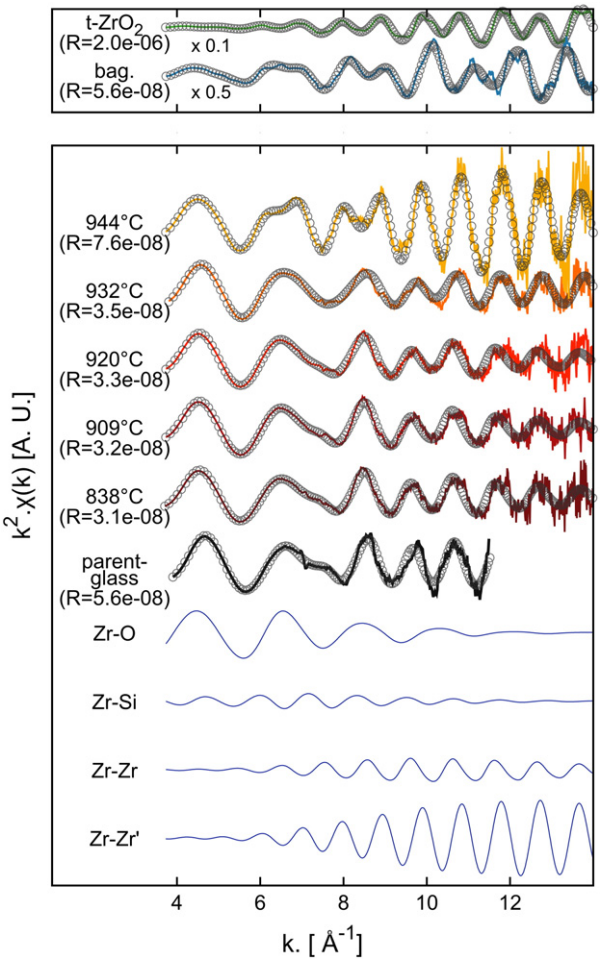

Fig. 5. Zr K-edge EXAFS spectra, corrected from background and multiple-electron excitation. The sequence presented follows the same order as in Fig. 4. The four bottom curves are the individual contributions used in the model. At 7.5 $Å^{-1}$ is a residual contribution from the multiple-electron excitation at ~18,820 eV. Experimental data are in plain lines and fitted signals in circles.

Only the sample treated at 944 °C presents a noticeable modification of the EXAFS spectrum. A new Zr–Zr contribution at 3.65 Å is consistent with the edge-sharing distance at 3.62 Å observed in the high temperature ZrO_2 polymorphs. This contribution presents an intense signal due to the high scattering factor of Zr. This effect is enhanced by the small variance of the bond. The presence of a Zr–Si contribution suggests that only a few ZrO_2 crystals have been formed as seen by HRTEM. These two distinct Zr–Zr linkages may correspond to the contribution of Zr in the glassy matrix and crystalline ZrO_2. However, as EXAFS averages structural information, a mix of contribution has a limit

Table 2
Structural parameters resulting from the fit of the EXAFS spectra of the reference compounds.

A			Zr–O	Zr–Si(1)	Zr–Si(2)	Zr–Zr	Zr–Ca
Baghdadite	E_0 (eV)	CN	6	1	1	2	7
	18012.5	d (Å)	2.13	3.26	3.10	3.63	3.80
		Var. ($Å^2$)	0.006	0.001	0.004	0.002	0.016
		b					0.60
B				Zr–O	Zr–O		Zr–Zr
t-ZrO_2	E_0 (eV)	CN		4	4		12
	18,010	d (Å)		2.09	2.34		3.64
		Var. ($Å^2$)		0.001	0.013		0.005

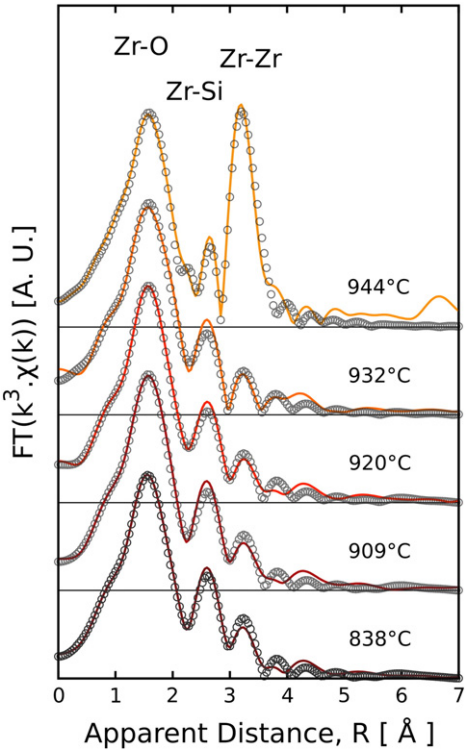

Fig. 6. Forward Fourier transform of the EXAFS signal (plain lines) and fit signal (circles). Apparent distances are given in Å.

of detection around 5%. The lack of evolution of the parent-glass model up to 932 °C and the very beginning of the detection of a crystalline Zr–Zr contribution at 944 °C shows that nucleation is probed at its very initial stages and only concerns a minor proportion of Zr.

4. Discussion

4.1. Role of Zr^{4+} as a nucleating agent

As shown by DSC, Zr^{4+} has a "nucleating" role in the MAS system by lowering all crystallization temperatures. Nucleating agents are sometimes described as "catalysts" [42] of the internal crystallization over volume crystallization. It has been shown that Ti, below 7–8 mol%. TiO_2, does not promote enough volume crystallization of the matrix and only surface crystallization occurs [43]. Although DSC alone does not allow to decipher matrix- vs surface-crystallization, the lowering of the temperature of the first matrix crystallization (1025 to 1015 °C) indicates that Zr^{4+} acts on the matrix crystallization mechanism at low content. On the other hand, nano-ZrO_2 appears in the bulk of the material (Fig. 2). The HRTEM images of the very first crystalline phases (Fig. 3) exhibit unambiguously the crystallization, at least in limited amount, of t-ZrO_2. These first nano-crystals could then form heterogeneous surfaces for subsequent crystallization of other phases, in a very high density, throughout the glass volume. Those two different pathways for the crystallization of the matrix, surface crystallization for Zr-free glass ceramic and bulk crystallization for Zr-containing glass-ceramics, are reflected by the shift of 30 °C on the fusion temperature that indicate two different microstructures. The crystallized nano-ZrO_2 cannot explain alone a lowering of fusion temperatures of all the crystals formed.

4.2. Structural role of Zr^{4+}

Zr^{4+} can generally adopt 3 coordination states in oxides: 6, 7 and 8 fold. Baghdadite represents the only known structure in which Zr^{4+}

Table 3
EXAFS-derived structural parameters for the parent-glass and glass-ceramics heated at temperatures ranging from 838 °C and 944 °C. Error analysis proceeded as [19], CN ± 0.5, R ± 0.01 Å, Var. ± 0.03 Å^2.

			Zr–O			Zr–Si			Zr–Zr			Zr–Zr		
	Edge (eV)	E_0 (eV)	CN	d (Å)	Var. (Å^2)	CN	d (Å)	Var. (Å^2)	CN	d (Å)	Var. (Å^2)	CN	d (Å)	Var. (Å^2)
Parent-glass	18,007.6	18,012	7.33	2.11	0.021	2.30	3.13	0.016	0.81	3.42	0.007	–	–	–
838 °C	18,012.9	18,012	7.50	2.11	0.020	2.23	3.12	0.013	0.90	3.41	0.009	–	–	–
909 °C	18,012.5	18,012	7.45	2.11	0.019	2.04	3.12	0.013	0.92	3.42	0.009	–	–	–
920 °C	18,010.4	18,012	7.19	2.12	0.018	2.28	3.12	0.015	0.75	3.42	0.009	–	–	–
932 °C	18,012.2	18,012	7.15	2.12	0.019	2.18	3.13	0.017	0.25	3.39	0.004	–	–	–
944 °C	18,007.5	18,012	6.89	2.12	0.017	0.71	3.11	0.004	1.01	3.33	0.012	1.08	3.65	0.004

forms pairs of edge-linked ZrO_6 octahedra [44]. The Zr–Si linkages in bagdhadite are by corners with two kinds of bonding [35]: one for which Zr–O–Si angle is closed and imposed a short Zr–Si distance, a second one with an open angle representative of the larger Zr–Si distances generally measured in glasses [12]. Higher coordination states of Zr^{4+} are encountered in several zirconium compounds. In the ZrO_2 polymorphs, the high temperature phase, c-ZrO_2, presents Zr^{4+} in 8-fold cubic coordination. At lower temperature, Zr^{4+} retains 8-fold coordination in t-ZrO_2, but the site is distorted due to an anti-symmetric displacement of the O neighbors, which gives two distinct Zr–O distances [37]. At low temperature, m-ZrO_2 results from a displacive transformation of t-ZrO_2 with a further distortion of the initial cubic coordination resulting in an irregular 7-fold coordination of Zr^{4+}. In zircon, $ZrSiO_4$, Zr is 8-fold coordinated, sharing edges with SiO_4 tetrahedron and Zr^{4+} polyhedron.

Both XANES and EXAFS data are in agreement with the presence of 7-fold Zr. This confirms previous findings on this system [13]. This site geometry represents a peculiar environment for Zr^{4+} at variance with the 6-fold geometry usually found in alkali silicate glasses [12,33,34]. These latter show a less intense pre-edge feature, indicating regular octahedral sites, as confirmed in the EXAFS functions by the presence of multiple scattering events [21].

The proposed model resulting from the EXAFS parameters (Table 3) is depicted in Fig. 7 and was obtained by considering interatomic distances, angles and steric effects. It shows that Zr^{4+} sites are connected to Si (Mg,Al) polyhedra. The inter-atomic distances of the different contributions are consistent with edge-sharing Zr and Si (Mg,Al) polyhedra (Fig. 7). Edge-sharing Zr–Si and Zr–Zr configurations are found in $ZrSiO_4$ and m-ZrO_2. This emphasizes the original surrounding of Zr in the parent-glass and glass-ceramics investigated in this study.

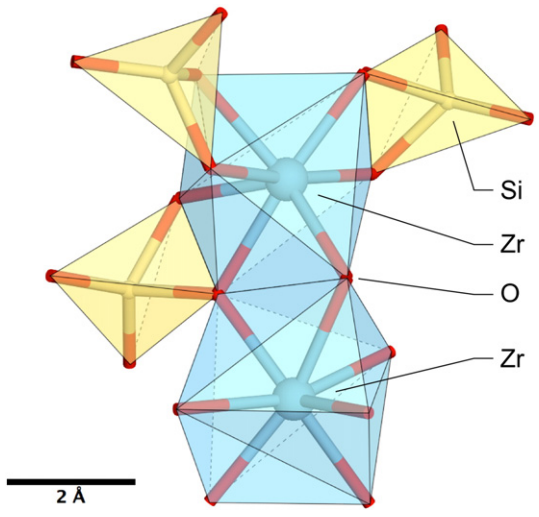

Fig. 7. Schematic structural model of Zr in the parent-glass. Zr atoms are in blue, Si (Al, Mg) atoms are in yellow and oxygen atoms are in red.

4.3. Evidence for organized Zr-enriched domains in the parent-glass

An important result from our EXAFS data is the presence of a Zr–Zr correlation at 3.40 Å, characterized by a low variance factor (Table 3). At 4 mol% ZrO_2, a statistical random distribution of Zr^{4+} would give an average Zr–Zr distance of about 11 Å, which is much larger than the experimental value. This suggests an inhomogeneous distribution of Zr^{4+} within the glass. Such an evidence of local organization within oxide glasses has already been shown for cations such as Ti or Ni [45,46]. This suggests that the inhomogeneous distribution of Zr corresponds to the formation of locally ordered domains. It is not possible to estimate the size and dimensionality of the domains enriched in Zr polyhedra. Moreover the Zr–Si contribution indicates that at least a part of the Zr^{4+} must be intimately associated with the aluminosilicate network. The presence of Zr–Zr linkages act as precursors in the formation of the ZrO_2 nano-crystals observed with TEM. Within EXAFS sensitivity to minor contributions, the local order seems conserved during the nucleation and the absence of modifications of the EXAFS spectra during the first steps of nucleation may indicate only limited rearrangements. Indeed, Zr-enriched zones can be rearranged at few °C above Tg as a result of a release of local stresses. This may lead to the formation of a periodical atomic arrangement, such as observed with TEM for t-ZrO_2. The environment of Zr^{4+} begins to evolve at 932° but it is only at 944 °C that it begins to change significantly with the appearance of a longer Zr–Zr distance to the signal of the parent matrix. This new contribution, sharp and with a small variance (Table 3), is related to a periodic ordering of the Zr^{4+} sites. As the probing of the nucleation is limited to the very first stages, the nature of these nano-crystals is difficult to determine accurately. XANES spectra are not consistent with the presence of bulk ZrO_2 (whether, monoclinic, tetragonal or cubic). Moreover, the crystal/matrix interface might contribute to deform the spectra of the nuclei nano-phases. A point that cannot be solved in our study is the composition and the possible doping of ZrO_2 nano-crystals by elements, such as Mg^{2+} or Al^{3+} ions.

Eventually, concerning the influence of the structural role of Zr^{4+} on the nucleation mechanism, ZrO_2 nano-crystals have been often invoked as activating centers for the formation of the silicate phases. An alternative mechanism could be that the formation of rearranged Zr-enriched domains and nano-ZrO_2 modify the structure of the remaining amorphous aluminosilicate network. Such rearrangement of the glassy part has been recently experimentally observed in a Ti-bearing MAS glass-ceramic [47]. This may favor the crystallization of β-quartz and then cordierite at lower temperature compared to the Zr-free glass.

5. Conclusion

Zr^{4+} acts as nucleating agent in $MgO–Al_2O_3–SiO_2–ZrO_2$ glass-ceramics. It promotes the crystallization of the matrix, lowering characteristic temperatures of thermal events. The Zr environment in the parent-glass corresponds to a 7-fold coordinated site, linked mainly with Si (Al,Mg) tetrahedra by edge sharing and forming

privileged bonds with other Zr^{4+} sites. Those pre-condensed bonds indicate an inhomogeneous distribution of Zr within the aluminosilicate network that can easily rearrange locally to form nano-ZrO_2. This early organization leads to a low activation energy in the formation of nano-sized ZrO_2 crystals just above Tg, and promotes the structural evolution of the matrix toward the crystallization of subsequent phases with increasing temperature.

Acknowledgements

IMPMC Transmission Electron Microscopy is supported by Region Ile De France (Convention SESAME 2000 E1435). Authors wish to acknowledge the help from Erick Lamotte in the synthesis of some glasses, Samuel Pierre for its help in the DSC measurements, Cécile Jousseaume for her help in the XANES and EXAFS acquisitions and helpful support (Saint-Gobain Recherche). Frédéric Wiss (Saint-Gobain ZIRPRO) and Michel Gaubil (Saint-Gobain SEVPRO) are also thanked for providing Y-doped t-ZrO_2.

References

[1] S.D. Stookey, Ind. Eng. Chem. 51 (1959) 805.
[2] P.W. McMillan, J. Non-Cryst. Solids 52 (1982) 67.
[3] W. Holand, V. Rbeallheinberger, M. Schweiger, Phil. Trans. R. Soc. Lond. Ser. A 361 (2003) 575.
[4] G.H. Beall, L.R. Pinckney, J. Am. Ceram. Soc. 82 (1999) 5.
[5] R. Tumala, J. Am. Ceram. Soc. 74 (1991) 895.
[6] P. Predecki, J. Haas, J. Faber Jr., R.L. Hitterman, J. Am. Ceram. Soc. 70 (1987) 175.
[7] A. Nandi, J. Am. Ceram. Soc. 82 (1999) 789.
[8] A. Ramos, M. Gandais, J. Cryst. Growth 100 (1990) 471.
[9] W. Bras, G. Greaves, M. Overluisen, S. Clark, G. Eeckhaut, J. Non-Cryst. Solids 351 (2005) 2178.
[10] T. Dumas, A. Ramos, M. Grandais, J. Petiau, J. Mater. Sc. Lett. 4 (1985) 129.
[11] M. Guignard, L. Cormier, V. Montouillout, N. Menguy, D. Massiot, A.C. Hannon, J. Phys. Condens. Matter 21 (2009) 375107.
[12] L. Galoisy, E. Pélegrin, M. Arrio, P. Ildefonse, G. Calas, J. Am. Ceram. Soc. 82 (1999) 2219.
[13] O. Dargaud, G. Calas, L. Cormier, L. Galoisy, C. Jousseaume, G. Querel, M. Newville, J. Am. Ceram. Soc. 93 (2010) 342.
[14] W. Zdaniewski, J. Am. Ceram. Soc. 58 (1975) 7.
[15] G. Neilson, Discuss. Faraday Soc. 50 (1970) 145.
[16] A. Di Cicco, G. Aquilanti, M. Minicucci, E. Principi, N. Novello, A. Cognigni, L. Olivi, J. Phys. Conf. Ser. 190 (2009) 012043.
[17] A. Sidike, I. Kusachi, N. Yamashita, Phys. Chem. Miner. 32 (2006) 665.
[18] A. Di Cicco, Phys. B 208 & 209 (1995) 125.
[19] A. Filipponi, A. Di Cicco, Task Quaterly 4 (2000) 575.
[20] B. Teo, Exafs: basic principles and data analysis, Springer-Verlag, Berlin, 1986.
[21] G. Ferlat, L. Cormier, M.H. Thibaut, L. Galoisy, G. Calas, J.M. Delay, D. Ghaleb, Phys. Rev. B 73 (2006) 214207.
[22] A.G. Kochur, A.M. Naodlinsky, V.F. Demekhin, J. Phys. C8 (1986) 83.
[23] A. Filipponi, A. Di Cicco, Phys. Rev. A 52 (1995) 1072.
[24] T. Barry, J. Cox, R. Morrel, J. Mater. Sci. 13 (1978) 594.
[25] M. Conrad, J. Mater. Sci. 7 (1972) 527.
[26] L.R. Pinckney, J. Non-Cryst. Solids 255 (1999) 171.
[27] L.R. Pinckney, G.H. Beall, J. Non-Cryst. Solids 219 (1997) 219.
[28] I. Jung, S.A. Decterov, A.D. Pelton, J. Phase Equilib. Diffus. 25 (2003) 329.
[29] T. Dumas, J. Petiau, J. Non-Cryst. Solids 81 (1986) 201.
[30] W. Schreyer, J. Schairer, Am. Mineral. 47 (1962) 90.
[31] U. Martin, H. Boysen, F. Frey, Acta Cryst. B 49 (1993) 403.
[32] R. Wurth, F. Muñoz, M. Müller, C. Rüssel, Mater. Chem. Phys. 116 (2009) 433.
[33] F. Farges, G. Calas, Am. Mineral. 76 (1991) 60.
[34] F. Farges, S. Rossano, Eur. J. Mineral. 12 (2000) 1093.
[35] J.R. Plaisier, J. Jansen, R.A.G. de Graaff, D.J.W. Ijdo, J. Solid State Chem. 115 (1995) 464.
[36] G. Teufer, Acta Cryst. 15 (1962) 1187.
[37] P. Li, I.W. Chen, J.E. Penner-Hann, Phys. Rev. B 48 (1993) 10063.
[38] P. Li, I.W. Chen, J.E. Penner-Hahn, Phys. Rev. B 48 (1993) 10074.
[39] N.E. Brese, M. O'Keeffe, Acta Cryst. B 47 (1991) 192.
[40] R.M. Hazen, L.W. Finger, Am. Mineral. 64 (1979) 196.
[41] D.K. Smith, H.W. Newkirk, Acta Cryst. 18 (1965) 983.
[42] P.W. McMillan, in: J.P. Roberts, P. Popper (Eds.), Glass-ceramics, 2nd ed., Academic Press, New York, 1979.
[43] V.M. Fokin, E.D. Zanotto, J. Non-Cryst. Solids 246 (1999) 115.
[44] G.D. Ilyushin, V.A. Blatov, Acta Cryst. B 58 (2002) 198.
[45] L. Cormier, P.H. Gaskell, G. Calas, A.K. Soper, Phys. Rev. B 58 (1998) 11322.
[46] L. Cormier, S. Creux, L. Galoisy, G. Calas, P.H. Gaskell, Chem. Geol. 128 (1996) 77.
[47] M. Guignard, L. Cormier, V. Montouillout, N. Menguy, D. Massiot, A.C. Hannon, B. Beuneu, J. Phys.: Condens. Matter (accepted).